

# Mean-acoustic fields exerted on a subwavelength axisymmetric particle

Everton B. Lima<sup>1</sup> and Glauber T. Silva<sup>1, a</sup>

*Physical Acoustics Group, Instituto de Física, Universidade Federal de Alagoas, Maceió, AL 57072-970, Brazil*

(Dated: 29 June 2021)

The acoustic radiation force produced by ultrasonic waves is the “workhorse” of particle manipulation in acoustofluidics. Nonspherical particles are also subjected to a mean torque known as the acoustic radiation torque. Together they constitute *the mean-acoustic fields* exerted on the particle. Analytical methods alone cannot calculate these fields on arbitrarily shaped particles in actual fluids and no longer fit for purpose. Here, a semi-analytical approach is introduced for handling subwavelength axisymmetric particles immersed in an isotropic Newtonian fluid. The obtained mean-acoustic fields depend on the scattering coefficients that reflect the monopole and dipole modes. These coefficients are determined by numerically solving the scattering problem. Our method is benchmarked by comparison with the exact result for a subwavelength rigid sphere in water. Besides, a more realistic case of a red blood cell immersed in blood plasma under a standing ultrasonic wave is investigated with our methodology.

©2021 Acoustical Society of America. [<https://doi.org/DOI number>]

[XYZ]

Pages: 1–11

## I. INTRODUCTION

Acoustofluidics is extensively based on the acoustic radiation force<sup>1</sup> produced by ultrasonic waves to control and pattern micro/nanoparticles (cells, microorganisms, and viruses) in a liquid medium. Nonspherical particles are also accompanied by the acoustic radiation torque.<sup>2</sup> The time-averaged radiation force and torque are referred to as *the mean-acoustic fields* that drive the particle dynamics in most acoustofluidic settings.

The analytical solutions for the mean-acoustic fields depend, apart from the incoming wave, on the geometric shape<sup>3–15</sup> and material properties<sup>16–22</sup> of the particle. Moreover, the viscous<sup>23–26</sup> and thermodynamic<sup>27</sup> properties of the surrounding fluid can significantly change the mean-acoustic fields on the particle. The solutions mentioned above are found for particles with a simple geometric shape, such as spheres and spheroids. Generally, these solutions are derived with the multipole expansion and angular spectrum methods. The equivalence of these theoretical approaches have been demonstrated in Ref. 28.

The mean-acoustic fields exerted on particles with more elaborate geometries are usually obtained through numerical techniques such as the finite element<sup>29–31</sup> and boundary element<sup>32</sup> method. Nevertheless, numerical methods compute the mean-acoustic fields for a given spatial configuration (position and orientation) of the particle relative to the incoming wave. To determine the particle position and orientation versus time, the mean-

acoustic fields have to be re-calculated at each time step in the interval of interest. As a consequence, particle dynamics analysis in acoustofluidics might be a very intense computational task. We emphasize that such analysis is of fundamental importance for understanding and designing micro/nanorobots propelled by ultrasound.<sup>33</sup>

In acoustofluidics, subwavelength nonspherical particles, which are much smaller than the wavelength, have been conveniently modeled as small spheres mainly because they fit the simple analytical expressions of the radiation force<sup>34</sup> and torque.<sup>4</sup> obtained in the scattering dipole approximation. Recently, analytical results considering a subwavelength spheroidal particle were also derived in the dipole approximation.<sup>35</sup> We stress that a complete theoretical description of the mean-acoustic fields for subwavelength particles of arbitrary geometry in an actual fluids seems to be unattainable.

This article proposes a semi-analytical approach to describe the mean-acoustic fields interacting with an arbitrary axisymmetric particle in Newtonian thermoviscous fluids. The obtained fields are related to the pressure and fluid velocity of the incident wave and the coefficients of the monopole and dipole modes of the scattered waves. These coefficients are obtained from the projection of the scattered pressure onto the angular part of the corresponding mode (monopole and dipole). In turn, the scattered pressure is obtained via a finite element solver. The numerical part of our method is verified against the exact solution for a rigid spherical particle in a lossless fluid. Besides, we apply our method to compute the mean-acoustic fields exerted on a red blood cell by a standing plane wave in blood plasma. The results, such as trap location and spatial orientation of the RBC,

---

<sup>a</sup>gtomaz@fis.ufal.br

are in good agreement with previously reported experiments.

## II. PHYSICAL MODEL

### A. General assumptions

Consider a subwavelength axisymmetric particle, i.e., with rotational symmetry around its principal axis, in a fluid of density  $\rho_0$  and compressibility  $\beta_0$ . The particle scatters an incoming wave of pressure amplitude  $p_{\text{in}}$ , angular frequency  $\omega$ , wavelength  $\lambda$ , and wavenumber  $k$ .

In Fig. 1, we sketch the the acoustic scattering problem for an axisymmetric particle. The scattering is conveniently described concerning the right-handed reference frame  $O_{x_p y_p z_p}$  fixed in the geometric center of the particle (centroid), referred to as the p-frame. It is also useful to obtain the mean-acoustic fields in a fixed laboratory reference frame  $O_{xyz}$  (l-frame) attached to the particle's centroid. The cartesian unit vectors of both reference systems are denoted by  $\mathbf{e}_i$  and  $\mathbf{e}_{i_p}$ , with  $i = x, y, z$  and  $i_p = x_p, y_p, z_p$ . Since the particle is invariant under infinitesimal rotations around the  $z_p$  axis, we need two angles  $(\alpha, \beta)$ , known as the Euler angles, to transform a vector from the p-frame to the l-frame. The transformation structure is formed by two elementary rotations: a counterclockwise rotation of an angle  $\alpha$  around the  $z$  axis, followed by a counterclockwise rotation of an angle  $\beta$  around new  $y'$  axis—see Fig. 1. We thus introduce the rotation tensor as

$$\begin{aligned} \mathbf{R} = & \cos \alpha \cos \beta \mathbf{e}_x \mathbf{e}_{x_p} - \sin \alpha \mathbf{e}_x \mathbf{e}_{y_p} + \cos \alpha \sin \beta \mathbf{e}_x \mathbf{e}_{z_p} \\ & + \sin \alpha \cos \beta \mathbf{e}_y \mathbf{e}_{x_p} + \cos \alpha \mathbf{e}_y \mathbf{e}_{y_p} + \sin \alpha \sin \beta \mathbf{e}_y \mathbf{e}_{z_p} \\ & - \sin \beta \mathbf{e}_z \mathbf{e}_{x_p} + \cos \beta \mathbf{e}_z \mathbf{e}_{z_p}, \end{aligned} \quad (1)$$

where the product  $\mathbf{e}_i \mathbf{e}_{i_p}$  is a dyadic, which forms the standard basis of second rank tensors in the Euclidean space. The Euler angles are given in the intervals  $0 \leq \alpha < 2\pi$  and  $0 \leq \beta \leq \pi$ . We define the particle orientation in both the p-frame and l-frame as

$$\mathbf{e}_p = \mathbf{e}_{z_p}, \quad (2a)$$

$$\mathbf{e}_l = \mathbf{R} \cdot \mathbf{e}_{z_p} = \cos \alpha \sin \beta \mathbf{e}_x + \sin \alpha \sin \beta \mathbf{e}_y + \cos \beta \mathbf{e}_z, \quad (2b)$$

where the center dot represents the scalar product between a tensor and vector or two vectors. Note also in deriving Eq. (2b), we have used the expressions  $\mathbf{e}_i \mathbf{e}_{x_p} \cdot \mathbf{e}_{z_p} = \mathbf{e}_i \mathbf{e}_{y_p} \cdot \mathbf{e}_{z_p} = \mathbf{0}$ , and  $\mathbf{e}_i \mathbf{e}_{z_p} \cdot \mathbf{e}_{z_p} = \mathbf{e}_i$ . The inverse transformation from the l-frame to the p-frame is given in Appendix A.

We assume that the largest dimension of the particle, denoted by  $a$ , is much smaller than the wavelength,  $a \ll \lambda$ , the so-called long-wavelength approximation. To determine  $a$  for an axisymmetric particle, we first notice that the particle occupies region, given in spherical coordinates, by  $\Omega_p = \{(r_p, \theta_p, \varphi_p) | 0 \leq r_p \leq R_p(\theta_p), 0 \leq \theta_p \leq \pi, 0 \leq \varphi_p < 2\pi\}$ , with  $R_p$  being the radial distance to the particle surface  $S_p$ . The largest and smallest radial

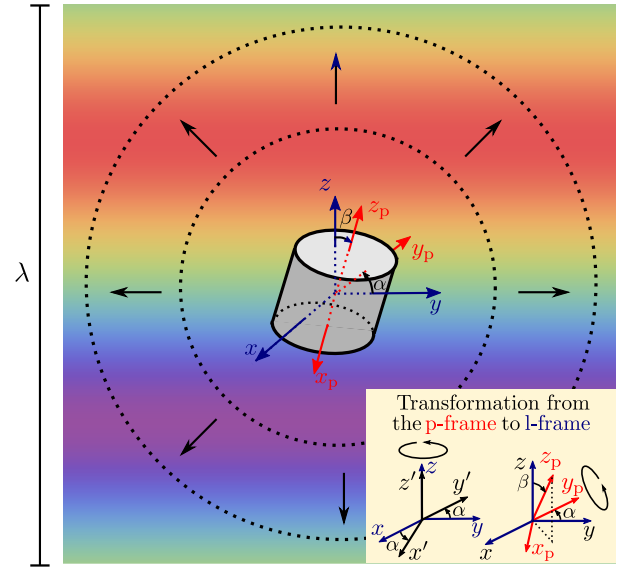


FIG. 1. Problem sketch: an incoming wave (background image with a positive and negative crest in purple and red, respectively) of wavelength  $\lambda$  is scattered by a small axisymmetric particle (gray cylinder). Two Euler angles  $(\alpha, \beta)$  describe the particle orientation regarding a laboratory frame denoted by blue axes. The particle frame is represented by red axes. The dotted concentric circles and black arrows denote the outgoing scattered wave. In the inset, we show the elementary rotations that map a vector from the particle frame (red axes) into the laboratory frame (blue axes).

distance to the particle surface are, respectively,

$$a = \max_{0 \leq \theta_p \leq \pi} R_p(\theta_p), \quad (3a)$$

$$b = \min_{0 \leq \theta_p \leq \pi} R_p(\theta_p). \quad (3b)$$

In case of a spherical particle,  $a = b$ . The characteristic size parameter of the subwavelength axisymmetric particle can be defined as

$$ka = \frac{2\pi a}{\lambda} \ll 1. \quad (4)$$

### B. Scattering normal modes

The scattered pressure by the particle is obtained by solving the Helmholtz equation with boundary conditions on the particle surface and the Sommerfeld radiation condition at the farfield ( $\mathbf{r}_p \rightarrow \infty$ ). The series solution represents the scattering pressure as an infinity sum of partial waves. It is convenient to express the partial waves in spherical coordinates  $(r_p, \theta_p, \varphi_p)$ . Hence, the  $n$ th-order partial wave is  $h_n(kr_p)Y_n^m(\theta_p, \varphi_p)$ , where  $h_n$  is the spherical Hankel function of first type,  $Y_n^m$  is the spherical harmonic,  $m$  is the number representing the wave orbital angular momentum. In the case of subwavelength particles much smaller than the wavelength, the

partial wave expansion can be truncated at the dipole-moment term ( $n = 1$ ). If we take a spherical particle as an example, we see that the truncation error is of the order of  $O[(ka)^2]$ .<sup>21</sup>

In the dipole approximation, the partial wave expansion of the scattering pressure is

$$p_{sc} = p_0 [a_{00}s_{00}Y_0^0(\theta_p, \varphi_p)h_0(kr_p) + [a_{1,-1}s_{1,-1}Y_1^{-1}(\theta_p, \varphi_p) + a_{10}s_{10}Y_1^0(\theta_p, \varphi_p) + a_{11}s_{11}Y_1^1(\theta_p, \varphi_p)]h_1(kr_p)], \quad (5)$$

where  $p_0$  and  $a_{nm}$  are the pressure amplitude and beam-shape coefficient of the incoming wave, respectively. We have four scattering coefficients representing the monopole ( $s_{00}$ ), transverse dipole ( $s_{1,-1}$ ) and ( $s_{11}$ ), and axial dipole ( $s_{10}$ ) modes. In Eq. (5), the time-dependent term  $e^{-i\omega t}$  is omitted for simplicity.

It is useful to introduce a function that represents the angular distribution of the  $(n, m)$  mode on a spherical surface of radius  $R > a$  and centered at the particle centroid,

$$p_{nm}(\theta_p, \varphi_p) = \frac{p_{sc}(kR, \theta_p, \varphi_p)}{p_0 a_{nm} h_n(kR)}. \quad (6)$$

Using the orthogonality of the spherical harmonics, the scattering coefficients are given as the projection of the normalized scattered pressure onto the corresponding angular mode,

$$s_{nm} = \langle n, m | p_{nm} \rangle = \int_0^{2\pi} d\varphi_p \int_0^\pi d\theta_p \sin \theta_p p_{nm}(\theta_p, \varphi_p) Y_n^{m*}(\theta_p, \varphi_p), \quad (7)$$

with asterisk denoting complex conjugation. The Dirac's bra-ket notation  $\langle | \rangle$  is used for simplicity.

In Appendix B, we show that the transverse dipole modes of an axisymmetric particle are degenerated,  $s_{1,-1} = s_{11}$ . Thus, the scattering coefficients of the problem are

$$s_{00} = \langle 0, 0 | p_{00} \rangle, \quad s_{10} = \langle 1, 0 | p_{10} \rangle, \quad s_{11} = \langle 1, 1 | p_{11} \rangle. \quad (8)$$

### C. Acoustic radiation force

The radiation force imparted on a subwavelength axisymmetric particle is given in terms of the scattering

coefficients and incident fields as<sup>35</sup>

$$\mathbf{F}_p^{\text{rad}} = \text{Re} \left[ \left( (\mathbf{e}_{x_p} \mathbf{e}_{x_p} + \mathbf{e}_{y_p} \mathbf{e}_{y_p}) \mathcal{D}_{x_p y_p} + \mathbf{e}_{z_p} \mathbf{e}_{z_p} \mathcal{D}_{z_p z_p} \right) \cdot \mathbf{v}_{\text{in},p}^* \right]_{\mathbf{r}_p=\mathbf{0}}, \quad (9a)$$

$$\mathcal{D}_{x_p y_p} = -\frac{2\pi i}{k^2} \left[ \frac{3\rho_0}{k} (s_{11} \mathbf{v}_{\text{in},p} \cdot \nabla_{x_p y_p} + s_{10} v_{\text{in},z_p} \partial_{z_p}) - i s_{00} (1 + 2s_{11}^*) \frac{p_{\text{in}}}{c_0} \right], \quad (9b)$$

$$\mathcal{D}_{z_p z_p} = -\frac{2\pi i}{k^2} \left[ \frac{3\rho_0}{k} (s_{11} \mathbf{v}_{\text{in},p} \cdot \nabla_{x_p y_p} + s_{10} v_{\text{in},z_p} \partial_{z_p}) - i s_{00} (1 + 2s_{10}^*) \frac{p_{\text{in}}}{c_0} \right]. \quad (9c)$$

where  $\mathbf{v}_{\text{in},p} = (v_{\text{in},x_p}, v_{\text{in},y_p}, v_{\text{in},z_p})$  is the fluid velocity regarding the p-frame, the asterisk denotes complex conjugation, and  $\nabla_{x_p y_p} = \mathbf{e}_{x_p} \partial_{x_p} + \mathbf{e}_{y_p} \partial_{y_p}$ . The acoustic fields should be evaluated at  $\mathbf{r}_p = \mathbf{0}$ . We should bear in mind that the acoustic fields in (9) correspond to the incoming wave for which thermoviscous effects can be neglected. Therefore, the lossless pressure-velocity relation

$$\mathbf{v} = -\frac{i\nabla p}{\rho_0 c_0 k} \quad (10)$$

is used into Eq. (9a) to obtain a simpler radiation force expression

$$\mathbf{F}_p^{\text{rad}} = \frac{1}{2} \text{Re} \left[ \beta_0 \boldsymbol{\alpha}_p^{(m)*} \cdot p_{\text{in}}^* \nabla_p p_{\text{in}} + \rho_0 \boldsymbol{\alpha}_p^{(d)*} \cdot \mathbf{v}_{\text{in},p}^* \cdot \nabla_p \mathbf{v}_{\text{in},p} \right]_{\mathbf{r}_p=\mathbf{0}}, \quad (11)$$

where  $\nabla_p = \mathbf{e}_{x_p} \partial_{x_p} + \mathbf{e}_{y_p} \partial_{y_p} + \mathbf{e}_{z_p} \partial_{z_p}$ , and

$$\boldsymbol{\alpha}_p^{(m)} = -\frac{4\pi i}{k^3} s_{00} [\mathbf{I} + 2s_{11}^* (\mathbf{e}_{x_p} \mathbf{e}_{x_p} + \mathbf{e}_{y_p} \mathbf{e}_{y_p}) + 2s_{10}^* \mathbf{e}_{z_p} \mathbf{e}_{z_p}], \quad (12a)$$

$$\boldsymbol{\alpha}_p^{(d)} = -\frac{12\pi i}{k^3} [s_{11} (\mathbf{e}_{x_p} \mathbf{e}_{x_p} + \mathbf{e}_{y_p} \mathbf{e}_{y_p}) + s_{10} \mathbf{e}_{z_p} \mathbf{e}_{z_p}] \quad (12b)$$

are the monopole and dipole acoustic polarizability tensors (in units of volume) of the particle, and  $\mathbf{I} = \mathbf{e}_{x_p} \mathbf{e}_{x_p} + \mathbf{e}_{y_p} \mathbf{e}_{y_p} + \mathbf{e}_{z_p} \mathbf{e}_{z_p}$  is the unit tensor. Note that the radiation force in Eq. (11) can also be understood in terms of the scattered and absorbed power by the particle in the dipole approximation (see Refs. 36–39).

After deriving the radiation force in the p-frame, we can obtain the equivalent expression in the l-frame. Using the rotational tensor described in Eq. (1), we find

$$\mathbf{F}^{\text{rad}} = \mathbf{R} \cdot \mathbf{F}_p^{\text{rad}} \quad (13)$$

Using Eq. (A2b) into this equation, we arrive at

$$\mathbf{F}^{\text{rad}} = \frac{1}{2} \text{Re} \left[ \beta_0 \boldsymbol{\alpha}^{(m)*} \cdot p_{\text{in}}^* \nabla p_{\text{in}} + \rho_0 \boldsymbol{\alpha}^{(d)*} \cdot \mathbf{v}_{\text{in}}^* \cdot \nabla \mathbf{v}_{\text{in}} \right]_{r=0}, \quad (14a)$$

$$\boldsymbol{\alpha}^{(m)} = \mathbf{R} \cdot \boldsymbol{\alpha}_p^{(m)} \cdot \mathbf{R}^{-1}, \quad (14b)$$

$$\boldsymbol{\alpha}^{(d)} = \mathbf{R} \cdot \boldsymbol{\alpha}_p^{(d)} \cdot \mathbf{R}^{-1}, \quad (14c)$$

where  $\mathbf{v}_{\text{in}}$  is the fluid velocity in the l-frame. This exquisite expression describes the acoustic radiation force on a particle immersed in a Newtonian fluid concerning the l-frame. Thermoviscous effects in the particle and fluid can be accounted for by solving the scattering problem considering temperature fields and appropriate boundary conditions.<sup>27</sup> Importantly, Eq. (14) is a generalization of the canonical form of the radiation force derived for spherical particles.<sup>24,40</sup>

We now proceed to the radiation force analysis of stationary and traveling waves. As the pressure amplitude of a stationary wave is a real-valued function, we have,  $p_{\text{in}}^* \nabla p_{\text{in}} = (1/2) \nabla |p_{\text{in}}|^2$ . Also, from Eq. (10) we see that  $\mathbf{v}_{\text{in}}^* \cdot \nabla \mathbf{v}_{\text{in}} = (1/2) \nabla |\mathbf{v}_{\text{in}}|^2$ . Thereby, for a stationary wave, Eq. (14) reduces to a gradient force

$$\mathbf{F}^{\text{rad}} = \left( \text{Re} \left[ \boldsymbol{\alpha}^{(m)} \right] \cdot \nabla E_{\text{pot}} + \text{Re} \left[ \boldsymbol{\alpha}^{(d)} \right] \cdot \nabla E_{\text{kin}} \right)_{r=0} \quad (15)$$

This equation shows that the kinetic  $E_{\text{kin}} = \rho_0 |\mathbf{v}_{\text{in}}|^2 / 4$  and potential  $E_{\text{pot}} = \beta_0 |p_{\text{in}}|^2 / 4$  energy densities pumped into the fluid are transformed into the acoustic force of radiation through their gradient projection onto the real part of the particle polarizabilities.

A nearly ubiquitous stationary wave employed in acoustofluidic devices is a standing plane wave whose acoustic fields are

$$p_{\text{in}} = p_0 \cos[k(z + z_0)], \quad (16a)$$

$$\mathbf{v}_{\text{in}} = \frac{ip_0}{\rho_0 c_0} \sin[k(z + z_0)] \mathbf{e}_z, \quad (16b)$$

where  $z_0$  is the particle position relative to the pressure antinode at  $z = 0$ . Replacing (16) into Eq. (15), we obtain the radiation force as

$$\mathbf{F}^{\text{rad}} = F_0 \Phi \sin 2kz_0, \quad (17a)$$

$$F_0 = AE_0, \quad E_0 = \frac{1}{4} \beta_0 p_0^2, \quad (17b)$$

where  $E_0$  is the acoustic energy density, and  $F_0$  is the characteristic force. The characteristic area  $A$  can be either the axial ( $A_{\parallel}$ ) and transverse ( $A_{\perp}$ ) particle cross-

section area. The acoustophoretic vector is expressed by

$$\begin{aligned} \Phi &= \frac{k}{A} \text{Re} \left[ \boldsymbol{\alpha}^{(m)} - \boldsymbol{\alpha}^{(d)} \right] \cdot \mathbf{e}_z \\ &= \frac{2\pi}{k^2 A} \cos \alpha \sin 2\beta \text{Re} [3i(s_{10} - s_{11}) - 2is_{00}(s_{10}^* - s_{11}^*)] \mathbf{e}_x \\ &+ \frac{2\pi}{k^2 A} \sin \alpha \sin 2\beta \text{Re} [3i(s_{10} - s_{11}) - 2i(s_{10}^* - s_{11}^*)] \mathbf{e}_y \\ &+ \frac{4\pi}{k^2 A} \text{Re} [3i(s_{10} \cos^2 \beta + s_{11} \sin^2 \beta) - is_{00}(1 + 2s_{10}^* \cos^2 \beta \\ &+ 2s_{11}^* \sin^2 \beta)] \mathbf{e}_z. \end{aligned} \quad (18)$$

We see the radiation force depends on the particle orientation angles  $\alpha$  and  $\beta$ . In this regard, we shall see later that the possible equilibrium configurations are the axial ( $\beta = 0$ ) and transverse orientation ( $\beta = \pi/2$ ). In either orientation, the radiation force becomes an axial force,

$$\mathbf{F}^{\text{rad}} = F_0 \Phi \sin 2kz_0 \mathbf{e}_z, \quad (19)$$

where  $\Phi$  jointly represents the axial  $\Phi_{\parallel}$  and transverse  $\Phi_{\perp}$  acoustophoretic factors. They are expressed by

$$\Phi_{\parallel} = \frac{4\pi}{k^2 A_{\parallel}} \text{Re} [3is_{10} - is_{00}(1 + 2s_{10}^*)], \quad (\beta = 0), \quad (20a)$$

$$\Phi_{\perp} = \frac{4\pi}{k^2 A_{\perp}} \text{Re} [3is_{11} - is_{00}(1 + 2s_{11}^*)], \quad (\beta = \pi/2). \quad (20b)$$

The position where the particle will be trapped depends on the sign of  $\Phi$ . The trap is located in a pressure node if  $\Phi > 0$ , and in a pressure antinode, otherwise. For a spherical particle, the axial and transverse dipole modes are degenerate  $s_{10} = s_{11}$ —see Eq. (37). Hence, the axial and transverse acoustophoretic factors equalize,  $\Phi_{\parallel} = \Phi_{\perp}$ . This result is also in agreement with previously obtained solutions.<sup>4,34,41</sup> The equations in (20) also agree with the analytical expressions derived for a prolate spheroidal particle.<sup>6</sup>

Now we focus our analysis on a traveling plane wave with pressure and velocity fields given by

$$p_{\text{in}} = p_0 e^{ikz}, \quad (21a)$$

$$\mathbf{v}_{\text{in}} = \frac{p_0}{\rho_0 c_0} e^{ikz} \mathbf{e}_z. \quad (21b)$$

In this particular case, the radiation force in Eq. (14a) becomes

$$\begin{aligned} \mathbf{F}^{\text{rad}} &= F_0 \Phi, \\ \Phi &= -\frac{2k}{A} \text{Im} \left[ \left( \boldsymbol{\alpha}^{(\text{m})} + \boldsymbol{\alpha}^{(\text{d})} \right) \cdot \mathbf{e}_z \right] \\ &= \frac{4\pi}{k^2 A} \cos \alpha \sin 2\beta \text{Re}[3(s_{10} - s_{11}) + 2s_{00}(s_{10}^* - s_{11}^*)] \mathbf{e}_x \\ &\quad + \frac{4\pi}{k^2 A} \sin \alpha \sin 2\beta \text{Re}[3(s_{10} - s_{11}) + 2s_{00}(s_{10}^* - s_{11}^*)] \mathbf{e}_y \\ &\quad + 8\pi \text{Re}[3(s_{10} \cos^2 \beta + s_{11} \sin^2 \beta) + s_{00}(1 + 2s_{10}^* \cos^2 \beta \\ &\quad + 2s_{11}^* \sin^2 \beta)] \mathbf{e}_z. \end{aligned} \quad (22)$$

Here the acoustophoretic vector is a result of the scattered and absorbed momentum fluxes.<sup>38,39</sup> The radiation force dependence with particle orientation is also noted. Again, the possible axial and transverse equilibrium orientations of the particle are  $\beta = 0, \pi/2$ , which leads to an axial radiation force,

$$\mathbf{F}^{\text{rad}} = F_0 \Phi \mathbf{e}_z. \quad (24)$$

The factor  $\Phi$  jointly represents

$$\Phi_{\parallel} = 8\pi \text{Re}[3s_{10} + s_{00}(1 + 2s_{10}^*)], \quad (\beta = 0), \quad (25a)$$

$$\Phi_{\perp} = 8\pi \text{Re}[3s_{11} + s_{00}(1 + 2s_{11}^*)], \quad (\beta = \pi/2). \quad (25b)$$

It is worth noticing that (25) covers previous results for a spherical particle.<sup>4,34,41</sup>

#### D. Acoustic radiation torque

The acoustic radiation torque  $\boldsymbol{\tau}_p^{\text{rad}}$  generated by an acoustic wave relative to the p-frame is expressed by<sup>11,35</sup>

$$\begin{aligned} \boldsymbol{\tau}_p^{\text{rad}} &= \frac{6\pi\rho_0}{k^3} \text{Im} \left[ \gamma_{\perp} (v_{\text{in},y_p} \mathbf{e}_{x_p} - v_{\text{in},x_p} \mathbf{e}_{y_p}) v_{\text{in},z_p}^* \right. \\ &\quad \left. + \gamma_{\parallel} v_{\text{in},x_p} v_{\text{in},y_p}^* \mathbf{e}_{z_p} \right]_{\mathbf{r}_p=0}, \end{aligned} \quad (26a)$$

$$\gamma_{\perp} = s_{10}^* + s_{11} + 2s_{11}s_{10}^*, \quad (26b)$$

$$\gamma_{\parallel} = s_{11} + s_{11}^* + 2|s_{11}|^2. \quad (26c)$$

The quantities  $\gamma_{\perp}$  and  $\gamma_{\parallel}$  are the transverse and axial gyroacoustic functions. To obtain the radiation torque in the l-frame, we first need to consider the velocity field relation

$$\mathbf{v}_{\text{in},p} = \mathbf{R}^{-1} \cdot \mathbf{v}_{\text{in}}. \quad (27)$$

Using MATHEMATICA software (Wolfram, Inc., USA), we insert Eq. (27) into Eq. (26a) and apply the rotational tensor to obtain

$$\begin{aligned} \boldsymbol{\tau}^{\text{rad}} &= \mathbf{R} \cdot \boldsymbol{\tau}_p^{\text{rad}} \\ &= \frac{6\pi\rho_0}{k^3} \text{Im} \left\{ \left[ \gamma_{\perp} (v_{\text{in},y} \cos \beta - v_{\text{in},z} \sin \alpha \sin \beta) (v_{\text{in},x}^* \cos \alpha \sin \beta + v_{\text{in},y}^* \sin \alpha \sin \beta + v_{\text{in},z}^* \cos \beta) \right. \right. \\ &\quad + \gamma_{\parallel} \cos \alpha \sin \beta (v_{\text{in},y}^* \cos \alpha - v_{\text{in},x}^* \sin \alpha) (v_{\text{in},x} \cos \alpha \cos \beta + v_{\text{in},y} \sin \alpha \cos \beta - v_{\text{in},z} \sin \beta) \mathbf{e}_x \\ &\quad + [\gamma_{\parallel} \sin \alpha \sin \beta (v_{\text{in},y}^* \cos \alpha - v_{\text{in},x}^* \sin \alpha) (v_{\text{in},x} \cos \alpha \cos \beta + v_{\text{in},y} \sin \alpha \cos \beta - v_{\text{in},z} \sin \beta) \\ &\quad - \gamma_{\perp} (v_{\text{in},x} \cos \beta - v_{\text{in},z} \cos \alpha \sin \beta) (v_{\text{in},x}^* \cos \alpha \sin \beta + v_{\text{in},y}^* \sin \alpha \sin \beta + v_{\text{in},z}^* \cos \beta) \mathbf{e}_y \\ &\quad + [\gamma_{\perp} \sin \beta (v_{\text{in},x} \sin \alpha - v_{\text{in},y} \cos \alpha) (v_{\text{in},x}^* \cos \alpha \sin \beta + v_{\text{in},y}^* \sin \alpha \sin \beta + v_{\text{in},z}^* \cos \beta) \\ &\quad \left. \left. + \gamma_{\parallel} \cos \beta (v_{\text{in},y}^* \cos \alpha - v_{\text{in},x}^* \sin \alpha) (v_{\text{in},x} \cos \alpha \cos \beta + v_{\text{in},y} \sin \alpha \cos \beta - v_{\text{in},z} \sin \beta) \mathbf{e}_z \right] \right\}_{\mathbf{r}=0}. \end{aligned} \quad (28)$$

We move on to analyze the acoustic radiation torque produced by a standing plane wave along the  $z$  axis as described in (16). With no transverse fluid velocity components,  $v_{\text{in},x} = v_{\text{in},y} = 0$ , the radiation torque in (28) becomes

$$\boldsymbol{\tau}^{\text{rad}} = \frac{3\pi\rho_0}{k^3} \text{Im}[\gamma_{\perp}] |v_{\text{in},z}|^2 \sin 2\beta \mathbf{e}_{\alpha}, \quad (29a)$$

$$\mathbf{e}_{\alpha} = \cos \alpha \mathbf{e}_y - \sin \alpha \mathbf{e}_x. \quad (29b)$$

The unit vector  $\mathbf{e}_{\alpha}$  is orthogonal to the particle axis of symmetry,  $\mathbf{e}_{\alpha} \cdot \mathbf{e}_1 = 0$ . Substituting Eq. (16b) into Eq. (29a) yields

$$\boldsymbol{\tau}^{\text{rad}} = \tau_0 \gamma_{\perp}^i \sin^2 k z_0 \sin 2\beta \mathbf{e}_{\alpha}, \quad (30a)$$

$$\tau_0 = V E_0, \quad \gamma_{\perp}^i = \frac{12\pi}{k^3 V} \text{Im}[\gamma_{\perp}], \quad (30b)$$

where  $\gamma_{\perp}^i$  is the transverse gyroacoustic parameter. In acoustofluidics, the typical characteristic torque scale is  $\tau_0 \sim 1 \text{ nN } \mu\text{m}$ .

As the particle will be trapped in either a pressure node or antinode, the pre-sine factor is reduced to one,  $\sin^2 kz_0 = 1$ . So the particle will be transversely aligned ( $\beta = \pi/2$ ) to the wave axis as the gyroacoustic parameter is positive,  $\gamma_{\perp}^i > 0$ . The axial orientation parallel to the wave axis ( $\beta = 0$ ) occurs as  $\gamma_{\perp}^i < 0$ .

Let us switch gears toward the radiation torque due to a traveling plane wave. By replacing Eq. (21b) into the radiation torque expression in (28), we find

$$\boldsymbol{\tau}^{\text{rad}} = \tau_0 \gamma_{\perp}^i \sin 2\beta \mathbf{e}_{\alpha}. \quad (31)$$

Apart from the pre-sine factor  $\sin^2 kz_0$ , this result is identical to the radiation torque by a standing wave given in Eq. (30a). Therefore, the particle orientation follows the same conclusion as the standing wave case.

### III. FINITE ELEMENT MODEL

To compute the scattering coefficients given in (8), we numerically solve the scattering of a traveling plane wave using the finite element (FE) method in the commercial software COMSOL Multiphysics (Comsol, Inc., USA). The choice for plane wave scattering is justified due to its simplicity and for having analytical expressions of the corresponding beam-shape coefficients. Once the scattering coefficients are determined, they can be used in conjunction with any incident wave. The p-frame is adopted in the finite element model. Besides, we use the *Acoustics Module* and *Solid Mechanics Module*, where the equations of linear acoustics and elastodynamics are implemented.

The pressure amplitude  $p_{\text{in}} = p_0 e^{i\mathbf{k} \cdot \mathbf{r}_p}$ , with wavevector  $\mathbf{k} = k(\sin \beta \mathbf{e}_{x_p} + \cos \beta \mathbf{e}_{z_p})$ , is set as the background pressure in the computational domain. To obtain the scattering coefficients in (8), we need the monopole and dipole beam-shape coefficients of a traveling plane wave,<sup>42</sup>

$$a_{00} = 2\sqrt{\pi}, \quad a_{10} = 2i\sqrt{3\pi} \cos \beta, \quad a_{11} = -i\sqrt{6\pi} \sin \beta. \quad (32)$$

For a rigid particle, the normal component of the fluid velocity should vanish at the particle surface  $S_0$ ,

$$(\mathbf{v}_{\text{in},p} + \mathbf{v}_{\text{sc},p})|_{\mathbf{r}_p \in S_0} \cdot \mathbf{n} = 0, \quad (33)$$

where  $\mathbf{v}_{\text{sc},p}$  is the scattered fluid velocity and  $\mathbf{n}$  is the outward normal vector of the particle. In the case of an elastic solid particle, the boundary conditions across the particle surface are the continuity of normal stresses and displacements, and zero tangential stress condition.

Accordingly, we have

$$(p_{\text{in}} + p_{\text{sc}} - \mathbf{n} \cdot \boldsymbol{\sigma}_p)|_{\mathbf{r}_p \in S_0} = 0, \quad (34a)$$

$$\mathbf{n} \cdot \left[ \frac{i}{\omega} (\mathbf{v}_{\text{in},p} + \mathbf{v}_{\text{sc},p}) - \mathbf{u}_p \right]_{\mathbf{r}_p \in S_0} = 0, \quad (34b)$$

$$\mathbf{t} \cdot \boldsymbol{\sigma}_p|_{\mathbf{r}_p \in S_0} = 0. \quad (34c)$$

where  $\mathbf{t}$  is the tangential unit vector,  $\boldsymbol{\sigma}_p$  and  $\mathbf{u}_p$  are the stress tensor and displacement vector inside the particle, respectively.

TABLE I: Geometrical and physical parameters used in the finite element simulations of the scattering problem.

Parameter	Description
Computational domain	Cylindrical
Diameter and height	100a
Radius of the integration surface ( $R$ )	5a/4
Minimum element size ( $e_{\text{min}}$ )	a/200
Maximum element size ( $e_{\text{max}}$ )	a/10 to a/3
Mesh growth rate	10 %
PML type	Polynomial
PML scaling factor	1
PML curvature parameter	2
PML thickness	50a
PML layers	30–50
Frequency	2–12 MHz
Fluid medium	Water
Mass density ( $\rho_0$ )	998 kg m <sup>-3</sup>
Compressibility ( $\beta_0$ )	0.4560 GPa <sup>-1</sup>
Particle	Rigid sphere
Radius ( $a$ )	3.91 $\mu\text{m}$
Fluid medium	Blood plasma <sup>43</sup>
Mass density ( $\rho_0$ )	1026 kg m <sup>-3</sup>
Compressibility ( $\beta_0$ )	0.4077 GPa <sup>-1</sup>
Particle	Red blood cell
Mass density <sup>43</sup> ( $\rho_p$ )	1100 kg m <sup>-3</sup>
Young's modulus <sup>44</sup> ( $E$ )	26 kPa
Compressibility <sup>43</sup> ( $\beta_p$ )	0.34 GPa <sup>-1</sup>
Geometric parameters: <sup>45</sup>	
Major semiaxis ( $a$ )	$R_0 = 3.91 \mu\text{m}$
Minor semiaxis ( $b$ )	$C_0/2 = 0.405 \mu\text{m}$
Constant $C_2$	7.83 $\mu\text{m}$
Constant $C_4$	-4.39 $\mu\text{m}$

The fluid domain corresponds to a mesh within a cylindrical region. We use a perfectly matched layer (PML) in a concentric cylindrical shell of a quarter-wavelength thickness to absorb the outgoing scattered wave, and thus avoid reflection back into the fluid do-

main. At the fluid-PML interface, the acoustic fields are continuous. The outer surface of the PML is a rigid wall.

To proceed with the FE modeling, we need to choose the appropriate mesh symmetry: 2D axisymmetric or 3D model. The 2D axisymmetric model is less computationally intense and corresponds to a plane wave propagating along the particle symmetry axis with  $\beta = 0$ . It can be used to compute the monopole ( $s_{00}$ ) and axial ( $s_{10}$ ) dipole coefficients only. The 2D mesh model is not suitable for computing the transverse dipole coefficient ( $s_{11}$ ), because  $\beta = 0$  implies  $a_{11} = 0$ , which leads to a not well-defined outcome of Eq. (6). We are, in principle, left with a full 3D scattering model to find  $s_{11}$ , which usually do not fit in low-memory computers ( $< 16$  GB). Nevertheless, the COMSOL FE solver transforms a 3D acoustic scattering by an axisymmetric object into a collection of 2D scattering problems using the built-in *Plane Wave Expansion* method.<sup>46</sup> We, therefore, use this method with five terms in the plane wave expansion to compute  $s_{11}$  with  $\beta = \pi/2$ . Here, the acoustic scattering by a rigid spherical particle and a red blood cell (RBC) is solved via the FE model. The simulation parameters used in the numerical solutions are presented in Table I.

In the upcoming analysis, the RBC is modeled as a solid elastic material with a biconcave disk-shaped geometry that is described in cylindrical coordinates  $(\varrho, \varphi, z)$  by the implicit equation<sup>45</sup>

$$z^2 = \frac{1}{4} \left[ 1 - \left( \frac{\varrho}{R_0} \right)^2 \right] \left[ C_0 + C_2 \left( \frac{\varrho}{R_0} \right)^2 + C_4 \left( \frac{\varrho}{R_0} \right)^4 \right]^2, \quad (35)$$

where  $2R_0$  and  $C_0$  are, respectively, the cell transverse diameter and central thickness, and  $C_2$ , and  $C_4$  are geometric parameters given in Table I.

Now we define the mesh convergence parameter as

$$\epsilon \equiv \max \left\{ \frac{|\operatorname{Re}[s_{nm}^{\text{ref}}] - \operatorname{Re}[s_{nm}]|}{|\operatorname{Re}[s_{nm}^{\text{ref}}]|}, \frac{|\operatorname{Im}[s_{nm}^{\text{ref}}] - \operatorname{Im}[s_{nm}]|}{|\operatorname{Im}[s_{nm}^{\text{ref}}]|} \right\}. \quad (36)$$

The reference solution  $s_{nm}^{\text{ref}}$  for the spherical particle is related to the exact coefficients given by

$$s_{00} = -\frac{j_0'(ka)}{h_0'(ka)}, \quad s_{10} = s_{11} = -\frac{j_1'(ka)}{h_1'(ka)}, \quad (37)$$

where  $j_n$  is the spherical Bessel function of order  $n$ , and the prime symbol means differentiation. Whereas for the RBC,  $s_{nm}^{\text{ref}}$  is the solution that shows negligible changes after further mesh refinements. The FE model was executed on a SUPERMICRO workstation (Supermicro Computer, Inc., USA) based in a dual-processor Intel Xeon E5-2690v2 @ 3 GHz and 224 GB memory size. The computational time is about 1 min in the 2D mesh and 5 min with the plane wave expansion method.

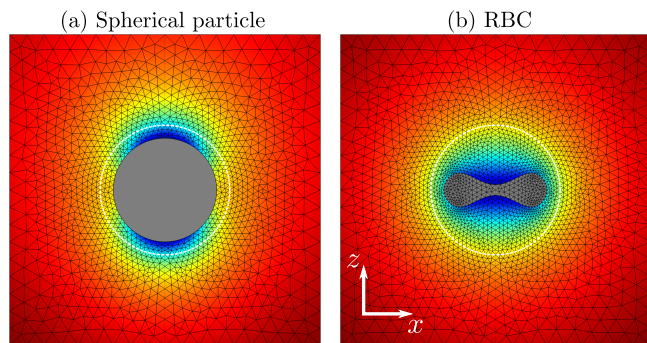


FIG. 2. The 2D axisymmetric mesh for the plane wave scattering by (a) a rigid spherical particle in water and (b) a RBC (modeled as an elastic solid) in blood plasma. The coarse mesh is for illustration purposes only. The particles, shown in gray, have the same diameter  $2a = 7.82 \mu\text{m}$ . The white dashed circle illustrates the integration surface; upon it, the scattering coefficients are computed. The plane wave travels in the vertical direction along the  $z$  axis. The background image corresponds to the real part of the computed scattered wave, where blue and red regions mean negative and positive pressures, respectively.

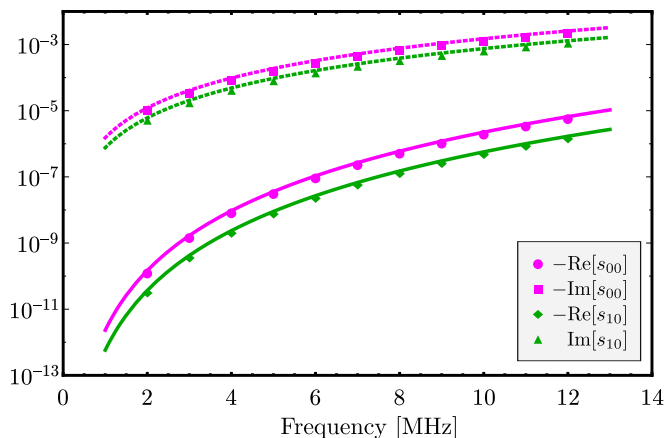


FIG. 3. The scattering coefficients of a rigid spherical particle much smaller than the wavelength. The solid and dashed lines are the corresponding exact solution from (37).

#### IV. RESULTS AND DISCUSSION

In Fig. 2, we depict the 2D axisymmetric mesh domain around the spherical particle and RBC. The particles have same diameter  $2a = 7.82 \mu\text{m}$ . The integration surface, where the scattering coefficients are computed, is shown as a white circle enclosing the particle. The real part of the scattered pressure is also illustrated as the background image. The positive and negative pressure correspond to blue and yellow-to-red regions, respectively.

In Fig 3, we plot scattering coefficients of the small rigid sphere in water for a routinely frequency range in

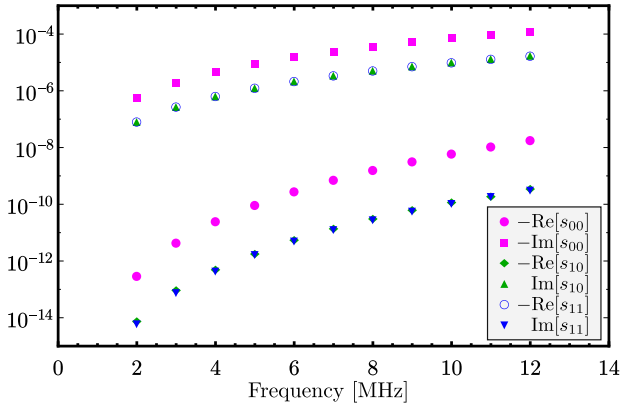


FIG. 4. The scattering coefficients of a RBC in blood plasma versus frequency.

acoustofluidics, 2–12 MHz. The numerical result is in excellent agreement with the exact solution. At 2 MHz, the convergence parameter is  $\epsilon = 7\%$ , with the maximum element size  $e_{\max} = a/3$ . This value drops to  $\epsilon = 1\%$  at 3 MHz, and keeps going down as the frequency increases. In our numerical studies, the solution convergence becomes an issue at frequencies smaller than 1 MHz. We also found that the transverse and axial dipole coefficients are degenerated,  $s_{11} = s_{10}$ , within the numerical error. We note that the convergence error as calculated from Eq. (36) is more prominent in the real part of the scattering coefficient, for which the reference solution is of the order  $s_{nm}^{\text{ref}} = O[(ka)^6]$ .<sup>21</sup> So, as the frequency decreases, the reference solution is drastically reduced, which may cause a convergence instability at lower frequencies.

Figure 4 shows the scattering coefficients of the RBC in blood plasma. In this study, the mesh convergence parameter is  $\epsilon < 9\%$ , for the maximum element size  $e_{\max} = a/10$ . The parameter approaches the upper bound at lower frequencies. With these coefficients, we can proceed to compute the radiation force and torque generated by a standing plane wave.

In Fig. 5, we show the computed gyroacoustic and acoustophoretic factors for the RBC. The obtained data is interpolated with polynomial functions of linear frequency  $f$ . Let us first examine the gyroacoustic factor. Referring to (30), we find

$$\gamma_{\perp}^i = -0.001433 - (0.000174 \text{ MHz}^{-1}) f, \quad (38)$$

in which the RBC volume<sup>45</sup>  $V = 94 \mu\text{m}^3$  was used, and the frequency should be specified in megahertz. The normalized root mean square error between the fitting polynomial and data is  $\text{nmrs} = 5\%$  (normalized to the data range). For a typical value of the energy density in acoustofluidics, say  $10 \text{ J m}^{-3}$ , the radiation torque peak is  $1.62 \text{ pN } \mu\text{m}$ . As  $\gamma_{\perp}^i$  is negative, we see the radiation torque aligns the RBC (axis of symmetry) with the axial direction ( $\beta = 0$ ). This prediction was experimentally observed in a half-wavelength acoustoflu-

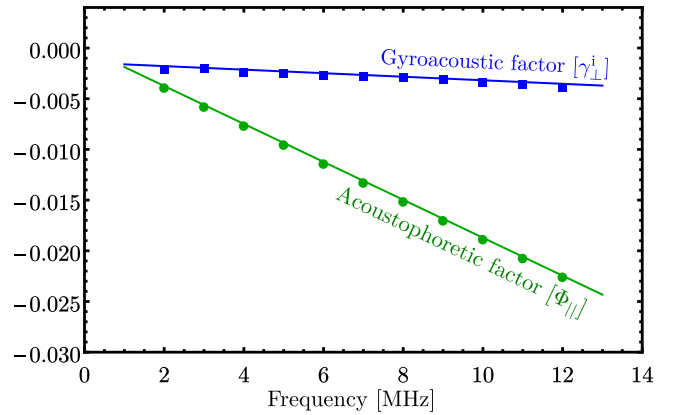


FIG. 5. The gyroacoustic and acoustophoretic factors of a RBC in blood plasma versus frequency. The green and blue lines represent a linear interpolation of data.

idic device.<sup>47</sup> Note also that when the second orientation angle is  $\alpha = 0$ , the radiation torque direction follows  $\boldsymbol{\tau}^{\text{rad}} \sim -\mathbf{e}_y$ . As the l-frame is a right-handed coordinate system, the RBC rotates around its transverse diameter ( $y$  axis) in the clockwise direction. On the other hand, when  $\alpha = \pi/2$  we have  $\boldsymbol{\tau}^{\text{rad}} \sim \mathbf{e}_x$ , the RBC rotates around its transverse diameter, but this time in counter-clockwise direction.

Having determined the RBC orientation, we know the radiation force by the standing wave is described by Eq. (19). Using a linear interpolator, we obtain the acoustophoretic factor as

$$\Phi_{\parallel} = -(0.001871 \text{ MHz}^{-1}) f. \quad (39)$$

where the transverse cross-section area  $A_{\perp} = \pi R_0^2$  was used, and the frequency should be given in megahertz. The interpolation error reads  $\text{nrms} = 0.1\%$ . The peak radiation force for  $E_0 = 10 \text{ J m}^{-3}$  and  $f = 2 \text{ MHz}$  is  $1.79 \text{ pN}$ . Moreover, as  $\Phi_{\parallel} < 0$ , we conclude the RBC is trapped in a pressure node,  $kz_0 = (2n + 1)\pi/2$ , with  $n \in \mathbb{Z}$ , which agrees with previous experimental observations.<sup>47</sup>

Finally, our results can be compared with those obtained by the Born approximation<sup>48</sup> for the RBC at 2 MHz, under the same conditions as specified in Table I. For the acoustic radiation force, the relative deviation between the results is a mere 0.4%. In the case of the radiation torque, we cannot, unfortunately, draw a comparison because the reference only provides the torque in a pressure antinode, e.g.,  $kd = 0$  in the article's notation. At this position, our method predicts a zero radiation torque. For the sake of curiosity, we calculate the peak torque from Ref. 48 as  $\sim 10^{-5}\tau_0$ . This value is two orders of magnitude smaller than our outcome for the RBC in a pressure node,

which can be considered close to our zero-torque prediction at a pressure antinode.



## V. SUMMARY AND CONCLUSIONS

This article introduces a semi-analytical method to compute the mean-acoustic fields (radiation force and torque) exerted on a subwavelength axisymmetric particle in a Newtonian fluid. The analytical part draws on the partial wave expansion of the scattering pressure up to the dipole approximation. The mean-acoustic fields are derived as a function of the scattering coefficients—see Eqs. (11) and (28). The monopole and dipole scattering coefficients are computed as the projection of the scattered pressure onto the angular part of the corresponding multipole mode—see Eq. (8). These coefficients are then numerically obtained using the finite element (FE) method to solve the plane wave scattering by the particle. We should remember that the scattering coefficients of spherical particles depend intrinsically on the mechanical properties of the particle and surrounding fluid, regardless the incoming ultrasonic wave. This can be seen, for instance, in the case of solid elastic particles.<sup>19</sup> In our approach, the scattering coefficient of axisymmetric particles are also independent of the incident wave—see Eq. (5). So, after obtaining these coefficients from the plane wave problem, one can compute the mean-acoustic fields on the particle caused by any structured wave generated in acoustofluidic devices, using Eqs. (14) and (28).

We performed numerical tests to obtain the scattering coefficients of a small rigid sphere in water. The results are in excellent agreement with the well-known exact scattering solution. The semi-analytical method is showcased for a RBC subjected to a standing plane wave in blood plasma. Our predictions for the particle orientation and entrapment location agree with previous experimental results.<sup>47</sup>

Lastly, our work is a concrete step toward computing the mean-acoustic fields on nonspherical particles in more realistic acoustofluidics settings. The method is valid for particles made of fluid, elastic, viscoelastic, and structured material. Besides, thermoviscous properties of the surrounding fluid can be incorporated into the numerical model. Not to mention that other numerical techniques such as the boundary element method, T-matrix, and finite differences can be used here. In conclusion, our theory may serve as the foundation for new investigations of RBCs and elongated cell dynamics in acoustofluidic devices and also the development of micro/nanorobots propelled by ultrasound.

## ACKNOWLEDGMENTS

We thank the Brazilian National Council for Scientific and Technological Development—CNPq, grant number 308357/2019-1.

## APPENDIX A:

The inverse rotational tensor, which transforms a vector from the l-frame to the p-frame, is given by

$$\begin{aligned} \mathbf{R}^{-1} = & \cos \alpha \cos \beta \mathbf{e}_{x_p} \mathbf{e}_x + \sin \alpha \cos \beta \mathbf{e}_{y_p} \mathbf{e}_x - \sin \beta \mathbf{e}_{z_p} \mathbf{e}_x \\ & - \sin \alpha \mathbf{e}_{x_p} \mathbf{e}_y + \cos \alpha \mathbf{e}_{y_p} \mathbf{e}_y - \cos \alpha \sin \beta \mathbf{e}_{x_p} \mathbf{e}_z \\ & + \sin \alpha \sin \beta \mathbf{e}_{y_p} \mathbf{e}_y + \cos \beta \mathbf{e}_{z_p} \mathbf{e}_z. \end{aligned} \quad (\text{A1})$$

The gradient operator is transformed as

$$\nabla = \mathbf{R} \cdot \nabla_p |_{r_p=r}, \quad (\text{A2a})$$

$$\nabla_p = \mathbf{R}^{-1} \cdot \nabla |_{r=r_p}. \quad (\text{A2b})$$

## APPENDIX B:

We want to demonstrate that the transverse dipole mode of axisymmetric particles are degenerated, e.g.,  $s_{11} = s_{1,-1}$ . Assume the plane wave travels along the  $x_p$  axis, then the wavevector is  $\mathbf{k} = k \mathbf{e}_{x_p}$  and  $\beta = \pi/2$ . We note the corresponding beam-shape coefficients are<sup>42</sup>  $a_{1,-1} = -a_{11} = i\sqrt{6}\pi$ . From Eq. (6), we see that the normalized pressure of the dipole mode satisfies  $p_{1,-1} = -p_{11}$ . Thus, using the spherical harmonic symmetry property  $Y_n^{-m} = (-1)^m Y_n^{m*}$  and referring to Eq. (7), we have

$$s_{1,-1} = \int_0^{2\pi} d\varphi_p \int_0^\pi d\theta_p \sin \theta_p p_{11}(\theta_p, \varphi_p) Y_1^1(\theta_p, \varphi_p). \quad (\text{B1})$$

Inasmuch as the particle rotation symmetry around  $z_p$  axis, the scattered pressure has to be an even function of the azimuthal angle  $\varphi_p$ . Hence  $p_{11}(\theta_p, -\varphi_p) = p_{11}(\theta_p, \varphi_p)$ , otherwise the scattered pressure will not be symmetric with respect to the  $x_p z_p$  plane as it should be. Equation (B1) can be re-written as

$$\begin{aligned} s_{1,-1} = & \int_0^{2\pi} d\varphi_p \int_0^\pi d\theta_p \sin \theta_p p_{11}(\theta_p, \varphi_p) Y_1^{1*}(\theta_p, \varphi_p) \\ = & \langle 1, 1 | p_{11} \rangle = s_{11}. \end{aligned} \quad (\text{B2})$$

Here  $Y_1^1(\theta_p, -\varphi_p) = Y_1^{1*}(\theta_p, \varphi_p)$  was used. We conclude the transverse dipole modes are indeed degenerated for axisymmetric particles.

<sup>1</sup>G. R. Torr, “The acoustic radiation force,” *Am. J. Phys.* **52**, 402–408 (1984).

<sup>2</sup>L. V. King, “On the theory of the inertia and diffraction corrections for the Rayleigh disc,” *Proc. Royal Soc. A* **153**, 17 (1935).

<sup>3</sup>L. Zhang and P. L. Marston, “Angular momentum flux of non-paraxial acoustic vortex beams and torques on axisymmetric objects,” *Phys. Rev. E* **84**(6), 65601 (2011).

<sup>4</sup>G. T. Silva, “Acoustic radiation force and torque on an absorbing compressible particle in an inviscid fluid,” *Journal of the Acoustical Society of America* **136**(5) (2014) doi: [10.1121/1.4895691](https://doi.org/10.1121/1.4895691).

<sup>5</sup>F. Nadal and E. Lauga, “Small acoustically forced symmetric bodies in viscous,” *Journal of the Acoustical Society of America* **139**, 1081 (2016).

- <sup>6</sup>G. T. Silva and B. W. Drinkwater, “Acoustic radiation force exerted on a small spheroidal rigid particle by a beam of arbitrary wavefront: Examples of traveling and standing plane waves,” *Journal of the Acoustical Society of America* **144**(5) (2018) doi: [10.1121/1.5080529](https://doi.org/10.1121/1.5080529).
- <sup>7</sup>L. Zhang, “Reversals of Orbital Angular Momentum Transfer and Radiation Torque,” *Phys. Rev. Applied* **10**, 34039 (2018).
- <sup>8</sup>Z. Gong, P. L. Marston, and W. Li, “*T*-matrix evaluation of three-dimensional acoustic radiation forces on nonspherical objects in Bessel beams with arbitrary order and location,” *Phys. Rev. E* **99**, 63004 (2019).
- <sup>9</sup>Z. Gong, P. L. Marston, and W. Li, “Reversals of Acoustic Radiation Torque in Bessel Beams Using Theoretical and Numerical Implementations in Three Dimensions,” *Phys. Rev. Applied* **11**, 64022 (2019).
- <sup>10</sup>T. S. Jerome, Y. A. Ilinskii, E. A. Zabolotskaya, and M. F. Hamilton, “Born approximation of acoustic radiation force and torque on soft objects of arbitrary shape,” *J. Acoust. Soc. Am.* **145**, 36 (2019).
- <sup>11</sup>J. H. Lopes, E. B. Lima, J. P. Leão-Neto, and G. T. Silva, “Acoustic spin transfer to a subwavelength spheroidal particle,” *Phys. Rev. E* **101**, 043102 (2020).
- <sup>12</sup>J. P. Leão-Neto, J. H. Lopes, and G. T. Silva, “Acoustic radiation torque exerted on a subwavelength spheroidal particle by a traveling and standing plane wave,” *Journal of the Acoustical Society of America* **147**(4) (2020) doi: [10.1121/10.0001016](https://doi.org/10.1121/10.0001016).
- <sup>13</sup>T. S. Jerome, Y. A. Ilinskii, E. A. Zabolotskaya, and M. F. Hamilton, “Acoustic radiation force on a compressible spheroid,” *Journal of the Acoustical Society of America* **148**, 2403 (2020).
- <sup>14</sup>Z. Gong and M. Baudoin, “Acoustic radiation torque on a particle in a fluid: An angular spectrum based compact expression,” *J. Acoust. Soc. Am.* **148**, 3131 (2020).
- <sup>15</sup>J. P. Leão-Neto, M. Hoyos, J.-L. Aider, and G. T. Silva, “Acoustic radiation force and torque on spheroidal particles in an ideal cylindrical chamber,” *Journal of the Acoustical Society of America* **149**, 285 (2021).
- <sup>16</sup>T. Hasegawa and K. Yosioka, “Acoustic-Radiation Force on a Solid Elastic Sphere,” *Journal of the Acoustical Society of America* **46**, 1139 (1969).
- <sup>17</sup>G. T. Silva, T. P. Lobo, and F. G. Mitri, “Radiation torque produced by an arbitrary acoustic wave,” *Europhysics Letters* **97**, 54003 (2012).
- <sup>18</sup>F. G. Mitri, T. P. Lobo, and G. T. Silva, “Axial acoustic radiation torque of a Bessel vortex beam on spherical shells,” *Phys. Rev. E* **85**(2), 26602 (2012).
- <sup>19</sup>D. Baresch, J.-L. Thomas, and R. Marchiano, “Three-dimensional acoustic radiation force on an arbitrarily located elastic sphere,” *J. Acoust. Soc. Am.* **133**, 25 (2013).
- <sup>20</sup>J. P. Leão-Neto, J. H. Lopes, and G. T. Silva, “Core-Shell Particles that are Unresponsive to Acoustic Radiation Force,” *Physical Review Applied* **6**(2) (2016) doi: [10.1103/PhysRevApplied.6.024025](https://doi.org/10.1103/PhysRevApplied.6.024025).
- <sup>21</sup>J. P. Leão-Neto and G. T. Silva, “Acoustic radiation force and torque exerted on a small viscoelastic particle in an ideal fluid,” *Ultrasonics* **71** (2016) doi: [10.1016/j.ultras.2016.05.018](https://doi.org/10.1016/j.ultras.2016.05.018).
- <sup>22</sup>G. T. Silva, J. H. Lopes, J. P. Leão-Neto, M. K. Nichols, and B. W. Drinkwater, “Particle Patterning by Ultrasonic Standing Waves in a Rectangular Cavity,” *Physical Review Applied* **11** (2019).
- <sup>23</sup>A. A. Doinikov, “Acoustic radiation pressure on a rigid sphere in a viscous fluid,” *Proceedings - Royal Society of London, A* **447**(1931), 447–466 (1994).
- <sup>24</sup>M. Settnes and H. Bruus, “Forces acting on a small particle in an acoustical field in a viscous fluid,” *Physical Review E* **85** (2012).
- <sup>25</sup>L. Zhang and P. Marston, “Acoustic radiation torque on small objects in viscous fluids and connection with viscous dissipation,” *J. Acoust. Soc. Am.* **136**, 2917–2921 (2014).
- <sup>26</sup>T. Baasch, A. Pavlic, and J. Dual, “Acoustic radiation force acting on a heavy particle in a standing wave can be dominated by the acoustic microstreaming,” *Phys. Rev. E* **100**, 61102 (2019).
- <sup>27</sup>J. T. Karlsen and H. Bruus, “Forces acting on a small particle in an acoustical field in a thermoviscous fluid,” *Phys. Rev. E* **93**, 043010 (2015).
- <sup>28</sup>Z. Gong and M. Baudoin, “Equivalence between angular spectrum-based and multipole expansion-based formulas of the acoustic radiation force and torque,” *J. Acoust. Soc. Am.* **149**, 3469 (2021).
- <sup>29</sup>P. Glynne-Jones, P. P. Mishra, R. J. Boltryk, and M. Hill, “Efficient finite element modeling of radiation forces on elastic particles of arbitrary size and geometry,” *The Journal of the Acoustical Society of America* **133**(4), 1885–1893 (2013) doi: [10.1121/1.4794393](https://doi.org/10.1121/1.4794393).
- <sup>30</sup>A. Garbin, I. Leibacher, P. Hahn, H. L. Ferrand, A. Studart, and J. Dual, “Acoustophoresis of disk-shaped microparticles: A numerical and experimental study of acoustic radiation forces and torques,” *J. Acoust. Soc. Am.* **138**, 2759 (2015).
- <sup>31</sup>T. Schwarz, P. Hahn, G. Petit-Pierre, and J. Dual, “Rotation of fibers and other non-spherical particles by the acoustic radiation torque,” *Microfluid Nanofluid* **18**, 65 (2015).
- <sup>32</sup>F. B. Wijaya and K.-M. Lim, “Numerical calculation of acoustic radiation force and torque acting on rigid Non-spherical particles,” *Acta Acust. united Ac.* **101**, 531 (2015).
- <sup>33</sup>W. Wang, L. A. Castro, M. Hoyos, and T. E. Mallouk, “Autonomous Motion of Metallic Microrods Propelled by Ultrasound,” *ACS Nano* **67**, 6122–6132 (2012).
- <sup>34</sup>L. P. Gor’kov, “On the forces acting on a small particle in an acoustic field in an ideal fluid,” *Sov. Phys.-Dokl.* **6**(9), 773–775 (1962).
- <sup>35</sup>E. B. Lima, J. P. Leão-Neto, A. S. Marques, G. C. Silva, J. H. Lopes, and G. T. Silva, “Nonlinear Interaction of Acoustic Waves with a Spheroidal Particle: Radiation Force and Torque Effects,” *Phys. Rev. Appl.* **13**, 064048 (2020).
- <sup>36</sup>L. Zhang and P. L. Marston, “Geometrical interpretation of negative radiation forces of acoustical Bessel beams on spheres,” *Phys. Rev. E* **84**, 35601 (2011).
- <sup>37</sup>F. G. Mitri and G. T. Silva, “Generalization of the extended optical theorem for scalar arbitrary-shape acoustical beams in spherical coordinates,” *Physical Review E* **90**(5) (2014) doi: [10.1103/PhysRevE.90.053204](https://doi.org/10.1103/PhysRevE.90.053204).
- <sup>38</sup>J. P. Leão-Neto, J. H. Lopes, and G. T. Silva, “Scattering of a longitudinal Bessel beam by a sphere embedded in an isotropic elastic solid,” *Journal of the Acoustical Society of America* **142**(5) (2017) doi: [10.1121/1.5009555](https://doi.org/10.1121/1.5009555).
- <sup>39</sup>J. H. Lopes, J. P. Leão-Neto, and G. T. Silva, “Absorption, scattering, and radiation force efficiencies in the longitudinal wave scattering by a small viscoelastic particle in an isotropic solid,” *Journal of the Acoustical Society of America* **142**, 2866–2872 (2017) doi: [10.1121/1.5009450](https://doi.org/10.1121/1.5009450).
- <sup>40</sup>I. D. Toftul, K. Y. Bliokh, M. I. Petrov, and F. Nori, “Acoustic Radiation Force and Torque on Small Particles as Measures of the Canonical Momentum and Spin Densities,” *Phys. Rev. Lett.* **123**, 183901 (2019).
- <sup>41</sup>H. Bruus, “Acoustofluidics 7: The acoustic radiation force on small particles” (2012), doi: [10.1039/c2lc21068a](https://doi.org/10.1039/c2lc21068a).
- <sup>42</sup>D. Colton and R. Kress, *Inverse Acoustic and Electromagnetic Scattering Theory*, 2nd ed. (Springer, Germany, 1998).
- <sup>43</sup>T. Gupta, R. Ghosh, and R. Ganguly, “Acoustophoretic separation of infected erythrocytes from blood plasma in a microfluidic platform using biofunctionalized, matched-impedance layers,” *Int J Numer Method Biomed Eng* **34**, e2943 (2018).
- <sup>44</sup>I. Dulińska, M. Targosz, W. Strojny, M. Lekka, P. Czuba, W. Balwierz, and M. Szymoński, “Stiffness of normal and pathological erythrocytes studied by means of atomic force microscopy,” *Biochem. Biophys. Methods* **66**, 1–11 (2006).
- <sup>45</sup>E. Evans and Y. C. Fung, “Improved measurements of the erythrocyte geometry,” *Microvascular Research* **4**(4), 335–347 (1972) doi: [10.1016/0026-2862\(72\)90069-6](https://doi.org/10.1016/0026-2862(72)90069-6).

- <sup>46</sup>COMSOL Inc., “Plane Wave Scattering off a 2D Axisymmetric Object: Plane Wave Expansion Approach” (2021), [www.comsol.com/model/plane-wave-scattering-off-a-2d-axisymmetric-object-plane-wave-expansion-approach-51311](http://www.comsol.com/model/plane-wave-scattering-off-a-2d-axisymmetric-object-plane-wave-expansion-approach-51311).
- <sup>47</sup>O. Jakobsson, M. Antfolk, and T. Laurell, “Continuous Flow Two-Dimensional Acoustic Orientation of Nonspherical Cells,”

- Anal. Chem. **86**, 6111–6114 (2014).
- <sup>48</sup>T. S. Jerome and M. F. Hamilton, “Acoustic radiation force and torque on inhomogeneous particles in the Born approximation,” Proc. Mtgs. Acoust. **39**, 45007 (2019).